Final Report for AASERT: Process Characterization of Non-Stoichiometric Material

Principle Investigators: April S. Brown and Gary May
School of Electrical and Computer Engineering
Microelectronics Research Center
Atlanta, GA 30332-0250

Abstract: This project addresses characterization of the Molecular Beam Epitaxy (MBE) process utilizing a Statistical Experiment Design (SED) approach and then building models. This approach is applied to GaAs-based materials, InP-based materials, and GaN-based materials, and to non-stoichiometric Be-doping InGaAs materials. The model responses are related to known physical effects for the growth of these materials. In addition, new phenomena are uncovered.

REPORT DOCUMENTATION PAGE

AFRL-SR-BL-TR-00-

0119

1. AGENCY USE ONLY (*Leave Blank*)	2. REPORT DATE	3. REPORT TYPE AND DATES COVERED
		FINAL REPORT -- June 1, 1996 through May 31, 1999

4. TITLE AND SUBTITLE
AASERT
Process Characterization of Non-Stoichiometric Material Growth

5. FUNDING NUMBERS
Contract Number:
F49620-96-1-0197

6. AUTHORS
April S. Brown

7. PERFORMING ORGANIZATION NAME(S) AND ADDRESS(ES)
Georgia Tech Research Corporation
Georgia Institute of Technology
Centennial Research Building, Room 246
Atlanta, GA 30332-0420

8. PERFORMING ORGANIZATION REPORT NUMBER
3

9. SPONSORING / MONITORING AGENCY NAME(S) AND ADDRESS(ES)
AFOSR (new address)
Dr. Gerald Witt
801 North Randolf Street
Arlington, VA 22203-1977

10. SPONSORING / MONITORING AGENCY REPORT NUMBER
FINAL TECHNICAL REPORT
W/SF 298

11. SUPPLEMENTARY NOTES

12a. DISTRIBUTION / AVAILABILITY STATEMENT

DISTRIBUTION STATEMENT A
Approved for Public Release
Distribution Unlimited

12b. DISTRIBUTION CODE

13. ABSTRACT *(Maximum 200 words)*

This project addresses characterization of the Molecular Beam Epitaxy (MBE) process utilizing a Statistical Experiment Design (SED) approach and then building models. This approach is applied to GaAs-based materials, InP-based materials, and GaN-based materials, and to non-stoichiometric Be-doping InGaAs materials. The model responses are related to known physical effects for the growth of these materials. In addition, new phenomena are uncovered.

14. SUBJECT TERMS	15. NUMBER OF PAGES 11
	16. PRICE CODE

17. SECURITY CLASSIFICATION OF REPORT	18. SECURITY CLASSIFICATION OF THIS PAGE	19. SECURITY CLASSIFICATION OF ABSTRACT	20. LIMITATION OF ABSTRACT

Project Summary:

Motivation: The goal of this project was to develop a systematic approach to Molecular Beam Epitaxy (MBE) experimentation and characterization. Such an approach has benefits to both research, in that experiments are made more efficient, and to technology transfer to manufacturing, in that a process methodology can be used. Our approach has been to perform statistical experiment designs (SEDs, also referred to as Design of Experiments, (DOE)) to uncover critical effects and interactions in the MBE process/ We then use this experimental data to build models.

The use of SED approach has the following benefits. First the approach is efficient; that is, the most information can be extracted from a limited number of experiments. Varying all of the factors simultaneously in the SED approach is better than the typical "one variable at a time" approach to experimentation. Using a SED allows for the development of process models that fully characterize the response surface, and finally, interactions between parameters can be uncovered.

In this project, we investigated four different types of materials grown by MBE and applied this approach to each type. These cases are discussed below.

Case I: AlGaAs-InGaAs Strained Quantum Well. This structure forms the basis of many important commercial devices grown by MBE today, including the PHEMT and the quantum well laser. A Resolution IV 2 6-2 fractional factorial design was used to analyze this structure. The structure and factor names and ranges are shown below in Figure 1.

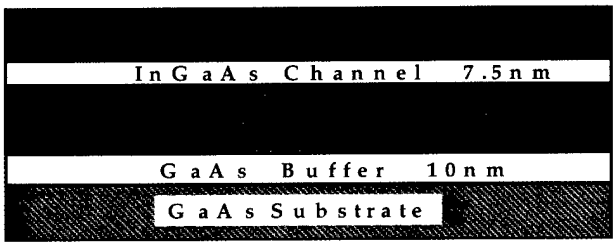

No	Factor Name	Range
1	Oxide Removal Temperature	580 - 650C
2	Time Duration for Oxide Rem	240 - 300 sec
3	AlGaAs Growth Temperature	580 - 630C
4	InGaAs Growth Temperature	450 - 520C
5	As Source Temperature	325 - 340C
6	Interrupt Time between Growth	30 - 90 sec

Figure 1: Structure and Factor Names and Ranges

Sixteen runs were made. For this design no main affects were aliased with any other main effects or any two-factor interactions. Characterization for this structure included X-Ray diffraction, photoluminescence and surface defect counts. Figure 2 shows the significant factors and interactions in relation to the characterization parameters (or outcomes of the runs).

		X-Ray			Photoluminesence			
	Defects	GaAs	AlGaAs		InGaAs		AlGaAs	
Factors		FWHM	FWHM	SEP	FWHM	Pos.	FWHM	Pos.
TOX	X	X	X	X	X	X	X	X
TI_OX	X		X	X		X		X
TAL	X	X		X		X		X
TIN	X			X	X			
PAS	X				X			
INT_TIME	X					X		
TOX*TAL			X					
TOX*TIN								
TOX*PAS			X	X			X	
TI_OX*TIN				X				
TI_OX*PAS				X				X
TAL*TIN				X			X	
TAL*PAS							X	X
TIN*PAS		X					X	X
TIN*INT_TIME	X					X	X	X
PAS*INT_TIME							X	X

Figure 2: Significant Factors and Interactions

Process models were developed using both response surface methods and neural networks. Figure 3 shows the InGaAs photolumuminscence full width at half-maximum (FWHM) vs. the quantum well growth temperature and the arsenic growth temperature (controlling the arsenic flux).

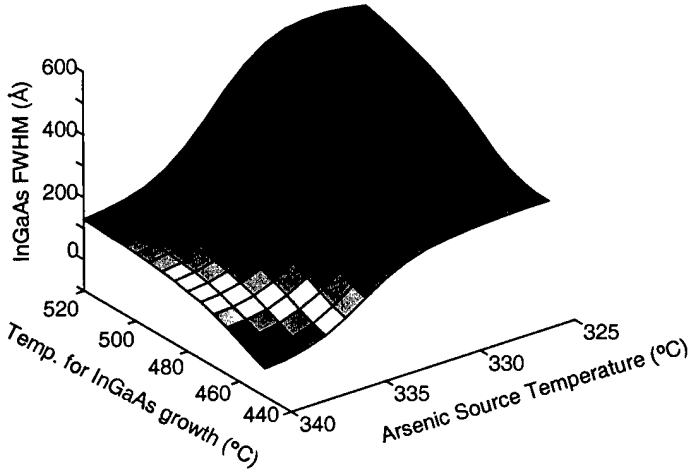

Figure 3. InGaAs Quantum Well FWHM vs. Substrate Temperature and Arsenic Pressure

This figure shows expected behavior. That is, the FWHM is narrower for those growth conditions that kinetically limit strain-induced degradation of a growing film. This observation confirms previous understanding of MBE growth of strained quantum wells. In addition, we have discovered new interactions. Figure 4 shows that the AlGaAs structural quality (as assessed by X-ray diffraction FWHM) depends on the temperature for substrate cleaning or oxide removal and the substrate temperature for growth.

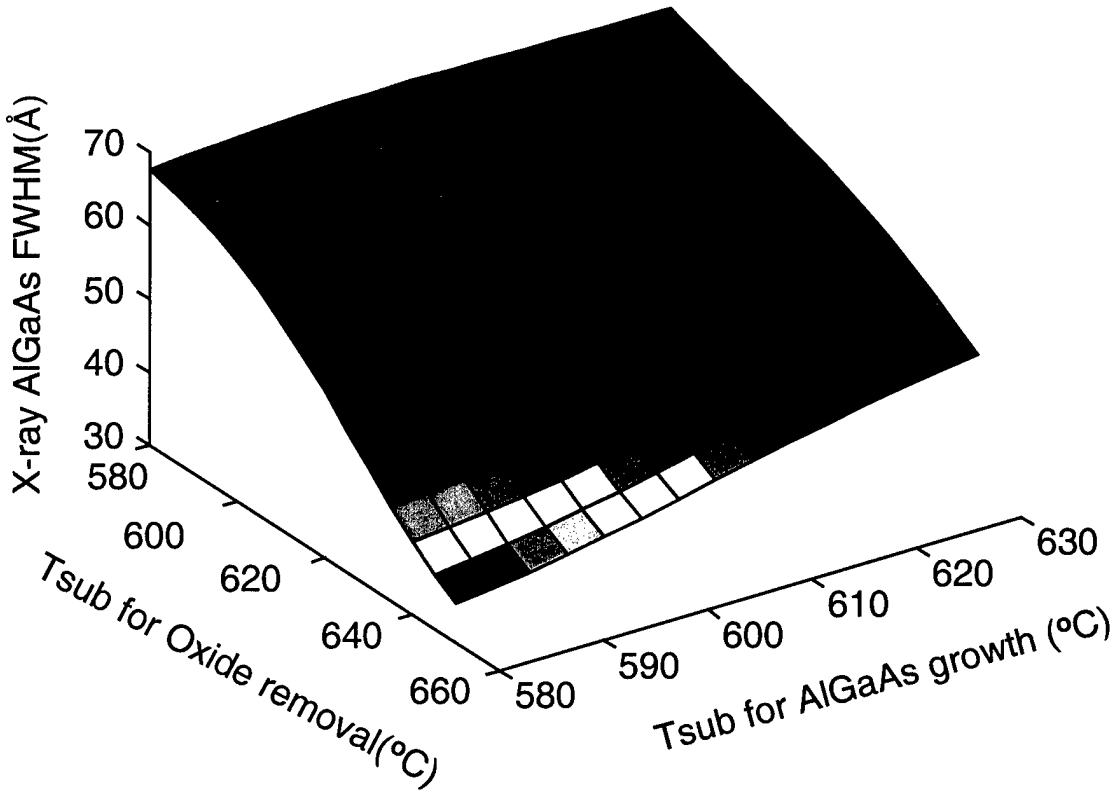

Figure 4: AlGaAs FWHM dependence on deoxidation temperature and substrate temperature

First, it is shown that if the higher the deoxidization temperature, the higher the structural film quality, and this probably results from oxygen incorporation into the film. In addition, the optimum substrate temperature depends on the oxide removal temperature. We conjecture that this is the result of interplay of cation migration and oxygen segregation and incorporation.

Case II. Case II is the growth of InP by solid source MBE. Solid source MBE is increasingly important as the growth technique of choice of P-containing materials. It avoids the toxicity issues inherent in the gas source methods and offers the advantages of MBE: low temperature growth and the resultant good interface quality and doping control. Three parameters were varied in this SED: P flux (from 4-8 x 10-6 T), the substrate temperature (from 470-540 C), and the growth rate (from 0.3-0.7 monolayers/sec). The experiment was conducted simultaneously on InP (100) and (111) substrates. The modeling was achieved by using a least squares estimation from RS/Discover software. Data analysis included Hall measurements and AFM for surface analysis. A wide range of conductivity was achieved for these undoped samples. The interactions between incident flux and growth temperature and growth rate relate primarily to impurity and

defect affects. For example, the P and In sources are both known sources of impurities, so that with increasing fluxes we can expect increasing impurity incorporation and resultant changes in electrical conductivity. In addition, the Group V/Group III flux and substrate temperature control the native defect concentrations (such as vacancies) and the desorption of impurities. Our experiment yielded 77K electron concentrations of 1.5 x 10^{15} cm^{-3} to 1.6 x 10^{16} cm^{-3}. Figures 5-7 show the model fits for interactions between the various parameters.

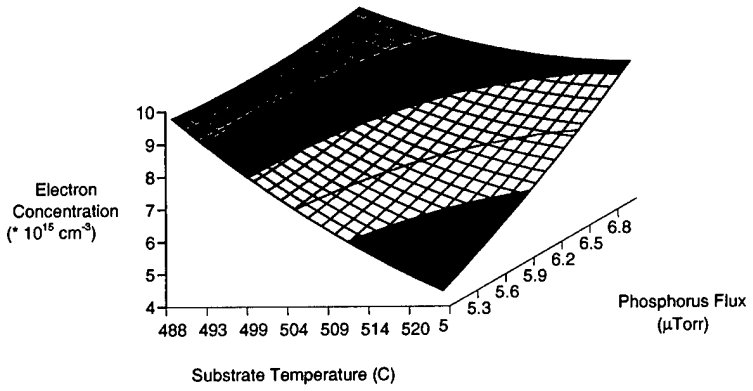

Figure 5: Electron concentration dependence on substrate temperature and phosphorus flux

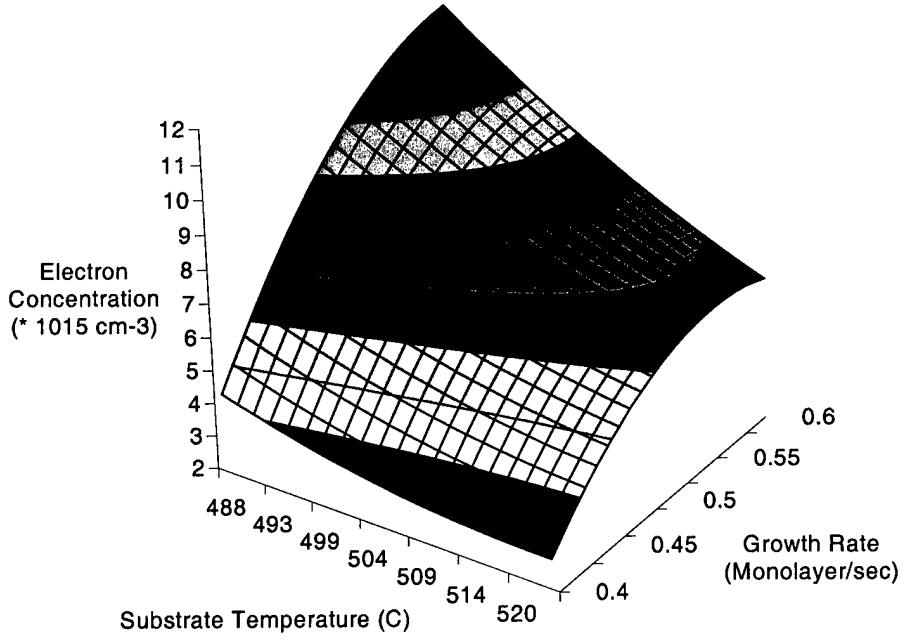

Figure 6: Electron concentration dependence on substrate temperature and growth rate

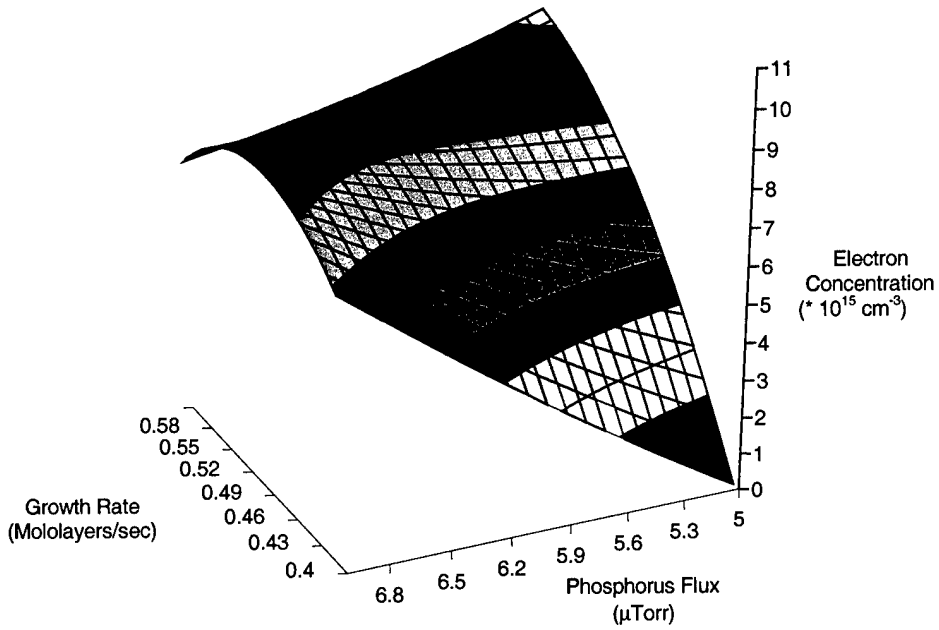

Figure 7: Electron concentration dependence on growth rate and phosphorus flux

Some general conclusions are made. First, a higher temperature results in a lower electron concentration. The interaction terms relate to appropriate V/III ratios for the given terms. We are still in the process of relating this model fit to our understanding of P-based growth.

Case III: Case III covers the important role of the low temperature buffer in the growth of GaN by MBE on sapphire. The buffer and nucleation conditions are known to establish the polarity of the film and the defect density (grain size) that can be propagated into the film. Figure 8 shows a schematic diagram of the structure growth.

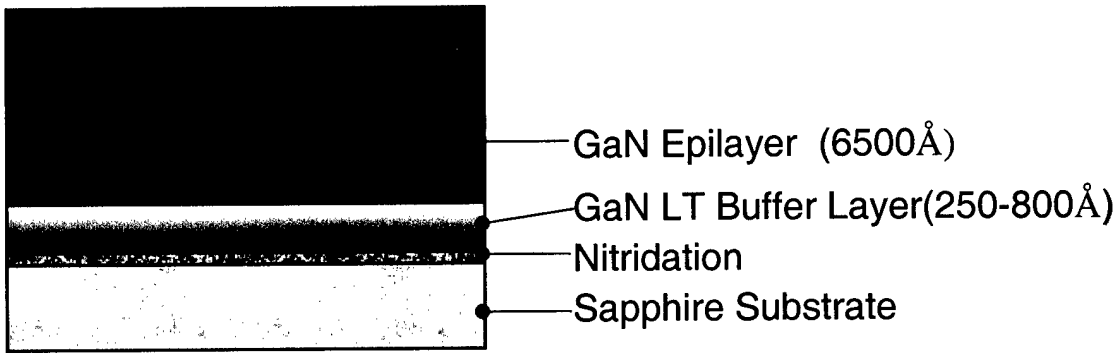

Figure 8: Structure of samples for GaN experiments

Table 1 shows the conditions varied in the buffer.

Layer	Factor	Range	Unit
Nitridation			
	Temperature	600 ~ 800	°C
	Time	1 ~ 30	min
Low Temperature Buffer Layer			
	Ga Flux	1.1 - 2.1x10^{-7}	Torr
	Growth Time	3 ~ 15	min
	Growth Temp.	400~600	°C
	Nitrogen Power	350 ~ 500	Watt
Epilayer			
	Ga Flux	4.4x10^{-7}	Torr
	Growth Time	120	min
	Growth Temp.	680	°C
	Nitrogen Power	450	Watt
	Nitrogen Pressure	2.2 x 10^{-5}	Torr

Table 1: Factors and ranges for the GaN experiment

The overlayer growth conditions were fixed. Table 2 shows the significant factors assessed from the material analysis.

	Photoluminescence				X-ray diffraction		Mobility		
	Linewidth (300K)	Peak to YL ratio	Linewidth (77K)	Peak to YL ratio	(00.4)	(10.5)	300K	77K	Thickness
NTime	0.6495	0.1417	**0.0036**	**0.0334**	0.1838	**0.0931**	0.1128	**0.0083**	0.9219
NTemp	0.3323	0.4109	0.6146	0.4637	0.5971	0.7226	0.7819	0.8105	0.1243
BTemp	0.3454	0.4375	**0.0510**	0.7333	0.3508	0.2082	0.3782	0.6461	0.5824
GaTemp	**0.0501**	**0.0480**	**0.0281**	**0.0243**	**0.0003**	**0.0039**	**0.0010**	**0.0012**	**0.0825**
NPower	**0.0218**	0.7545	0.3430	0.8515	0.3638	0.8505	0.4516	0.3809	0.1389
GTime	0.3852	0.3255	0.5066	0.1442	0.2536	0.4361	0.3868	**0.0872**	**0.0004**

Table 2: Significant factors (bold) for the experiments

Photolumisncesce, X-ray diffraction, mobility (of the films doped to 2 x 10^{18} cm^{-3}) were measured. In addition, correlations in the film properties were measured. The RHEED pattern was recorded at the termination of growth. It was found that a bulk, but streaky pattern correlates with the highest mobility. Films with reconstructed surfaces showed the lowest mobilities. This is shown in Figure 9.

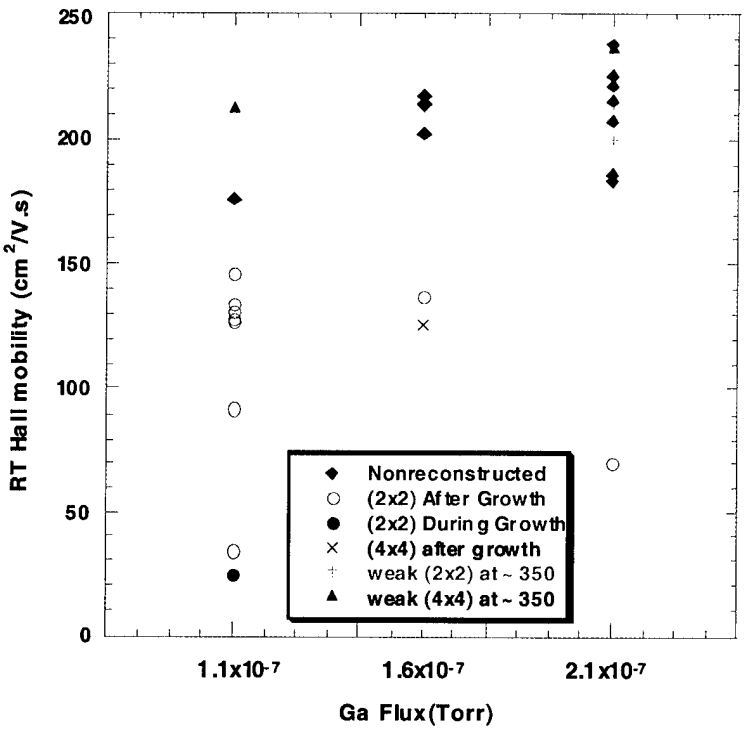

Figure 9: 300K Hall mobility vs. Ga flux (growth rate) and with RHEED pattern designation

We tried to assess the polarity of the films, but etching results were inconclusive. We conjecture that films with larger volumes of a single polarity are better than mixed polarity films, and that the reconstructions indicate domains of Ga-polarity. A uniform Ga-polarity would, of course, yield the best results. Figure 10 shows the dependence of the film mobility on the III/V flux ratio during the buffer growth.

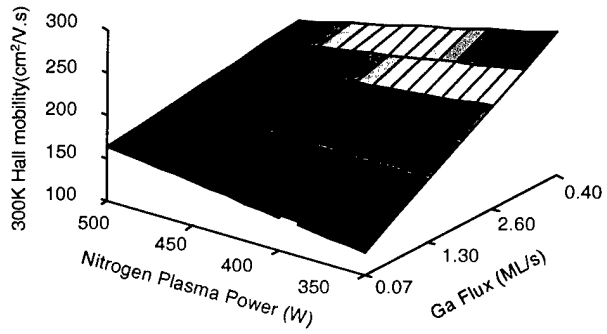

Figure 10: Dependence of 300K Hall mobility on buffer Ga flux (growth rate) and nitrogen plasma power

We find that a higher growth rate yields better mobility and that the higher N power probably induces some defects due to damage. A smoother surface is obtained with the higher growth rate as indicated by RHEED measured at the termination of the buffer (Figure 11).

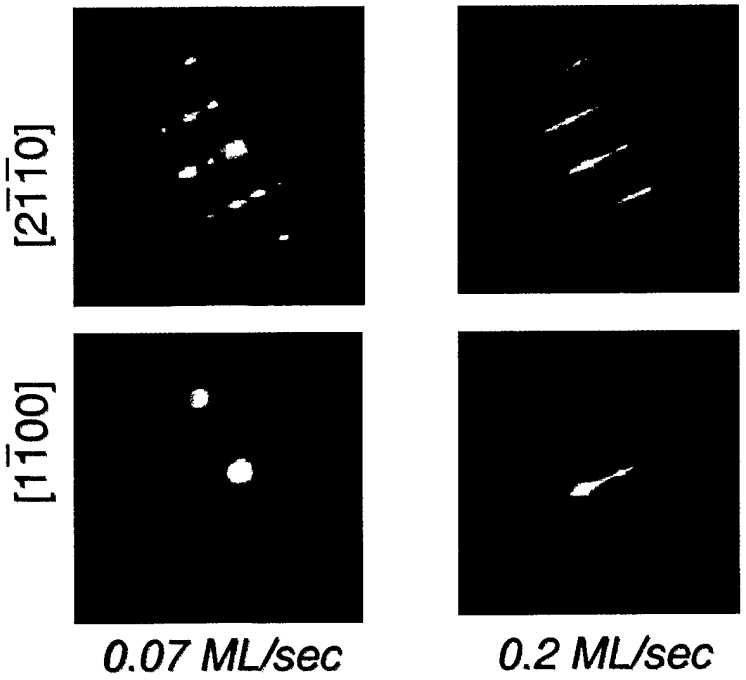

Figure 11. RHEED After Finishing Buffer Growth

This smoother surface translates to larger grain size in the final film morphology. Figure 12 shows AFM characterization of films with increasing growth rate and the corresponding mobilities.

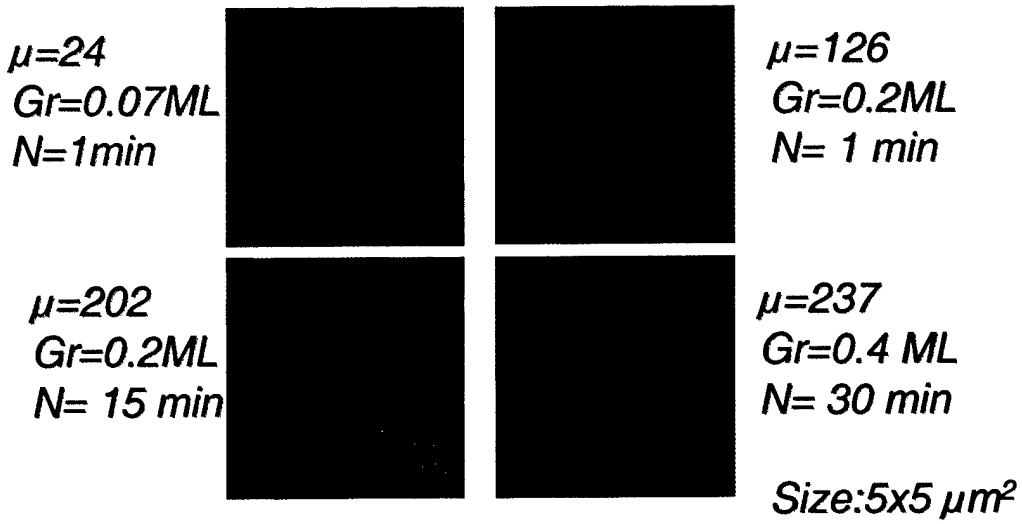

Figure: 12: AFM images of GaN surfaces with different buffer growth conditions

We continue to assess this data and this will serve as a launching point of further investigation.

Case IV: Case IV is a study of the growth and annealing conditions of low temperature InGaAs for high speed MSM applications (work pursued in collaboration with Professor Stephan Ralph). Three different process conditions were used for the growth. The growth temperatures were 225C, 350C or 450 C. The Be doping concentration was 3 x 10^{17} cm^{-3}, 2.5 x 10^{18} cm^{-3} to 1 x 10^{19} cm^{-3} and the As overpressures were either 15 x 10^{-6} T or 30 x 10^{-6} T. All the samples were analyzed as-grown and with 500 and 600 C anneals after growth. The photoexcited carrier lifetimes and the relative mobilities were determined via far infrared Terahertz spectroscopy. In addition, Hall measurements and linear absorption measurements were made. Models were made with neural networks. Carrier lifetimes from 800 to 1 psec were measured. It was confirmed that Be doping reduced the carrier lifetime for the as-grown materials. The shortest photoexcited carrier lifetimes were measured for the as-grown material with the highest Be doping and the lowest growth temperature. The use of a higher As overpressure increases the carrier lifetime independent of all other growth conditions. The carrier lifetimes are retained after the anneals for doping levels of 2.5 x 10^{18} cm^{-3} and 1 x 10^{19} cm^{-3}. For the Hall measurements, the lowest growth temperature produces n-type or highly resistive materials. Increasing the growth temperature is directly associated with increasing the hole concentration. This behavior is partially explained by the compensation effect of the donor. The carrier concentration is insensitive to the As overpressure. Figure 13 shows the measured carrier concentration vs. the growth conditions.

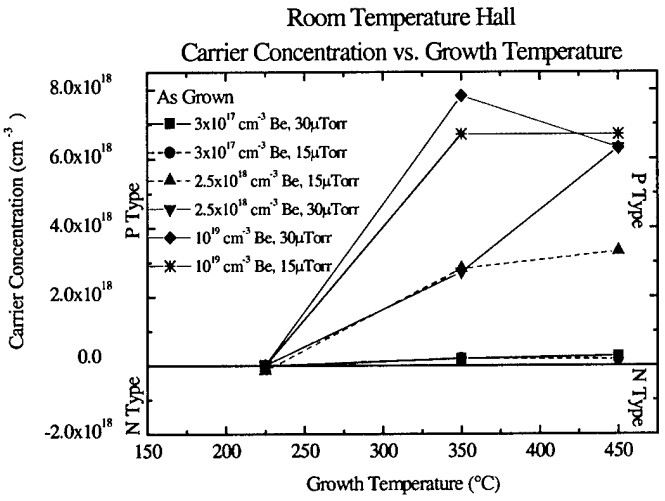

Figure 13: 300K Hall measurements for different growth conditions

The effect of annealing was very complex. The annealing behavior is highly sensitive to growth temperatures and Be concentration. Dramatic changes in lifetimes can be observed and are dependent on the As overpressure.

Conclusions: We have examined four cases for MBE growth and modeling using SED. We continue to expand our physical interpretations of the date. We are building on this work in

application to anion exchange (AFRL contract) and in application to device growth (NSF GOALI proposal is being planned with a company).

Publications:

1.K. Lee, T. Brown, G. Dagnall, R. Bicknell-Tassius, A. Brown, J. Dorsey and G. May, "Using Neural Networks to Build Models of Molecular Beam Epitaxy Suitable for Process Control Applications," IEEE Transactions on Semiconductor Manufacturing, 13(1) February 2000.
2.K. Lee, W. Doolittle, A. Brown, G. May and S. Stock, " The Role of Initial Growth Conditions on GaN Epitaxial Layers Grown by Molecular Beam Epitaxy," accepted for publication in Journal of Vacuum Science and Technology B, February 2000.
3.Ralph, S., Brown, A.S., Dagnall, G., Robert, Erik, and May, Gary, "Analysis of Be-doped LT InGaAs:Be," Electronic Materials Conference, Charlottesville, VA, June 1998.
4.Bicknell-Tassius, R., Brown, A.S., Lee, K., and May, G., "Application of Design of Experiments to InGaAs-GaAs Growth by MBE," Journal of Crystal Growth, 175/176, pp. 1131-1137, 1997.
5.Bicknell-Tassius, Robert, Lee, Kyeong, Brown, April S., Dagnall, Georgianna, and May, Gary, "The Growth of AlGaAs-InGaAs Quantum Well Structures by Molecular Beam Epitaxy: Observation of Critical Interdependent Effects," Applied Physics Letters, 70 (1), pp. 52-55, January 6, 1997.
6.Lee, K., Bicknell-Tassius, R., Dagnall, G., Brown, A., and May, G., "Statistical Experimental Design for MBE Process Characterization," Proceedings of the International Electronics Manufacturing Symposium, pp. 378-385, Dallas, TX, November 1996.
7.K. Lee, W.A. Doolittle, A. Brown, G. May and S. Stock, , " A comparative study of surface reconstruction of wurtzite GaN on (0001) sapphire by RF plasma-assisted molecular beam epitaxy,' submitted to Journal of Crystal Growth.

Graduate Students Supported on this Effort:

Terence Brown
Erik Roberts
Georgianna Dagnall